Publishing Excellence
Inspiring Progress
ARISTON PUBLICATIONS
MatSci Express
ISSN: 2997-8440 www.aristonpubs.com/matsci-express https://doi.org/10.69626/mse.2024.0069

RESEARCH ARTICLE

Selective Recognition of Lead and Cadmium in Potable Water Using Single Polypyrrole Nanowire Decorated with Cobalt Oxide Nanoparticles Electrode

Rahul S. Salunke [1], Yogesh Nakate [1], Ahmad Umar [2, 3, *], Amardip M. Patil [4], Umesh Nakate [5], Sotirios Baskoutas [6], Dhammanand J. Shirale [1, *]

ABSTRACT: The fabrication and characterization of a high-performance, robust, and highly sensitive sensor based on a single polypyrrole nanowire (sPpy NW) decorated with cobalt oxide nanoparticles (CoO_xNPs) for the selective recognition of lead (Pb^{2+}) and cadmium (Cd^{2+}) in potable water are described in this paper. The electrodeposition technique was used to prepare the sPpyNW/CoO_xNPs assembly, and square wave anodic stripping voltammetry (SW-ASV) was used to assess sensor performance. Optimizing sensor performance, such as deposition time, deposition potential, and supporting electrolyte, was used to assess for best sensor performance. The developed sensor exhibited excellent linearity and the linear range for the detection of individual Cd^{2+} and Pb^{2+} ions was determined to be 0.00 to 0.11 µM and 0.00 to 0.12 µM, respectively. The detection limits observed for both Pb^{2+} and Cd^{2+} sensors are 0.22 µM (R^2 = 0.9520) and 0.013 µM (R^2 = 0.9723), respectively. The linear range for the detection of Pb^{2+} and Cd^{2+} sensors present in the same sample was determined to be 0.00 to 0.09 µM, with a detection limit of 0.026 µM (R^2 = 0.8726) and 0.013 µM (R^2 = 0.9468) for Pb^{2+} and Cd^{2+}, respectively. The observed results revealed that the functionalization of CoO_xNPs on the surface of a sPpyNW electrode seems to be a very effective way of developing a sensitive, selective, and stable electrochemical sensor for Pb^{2+} and Cd^{2+}ions.

Keywords: Polypyrrole nanowire, Cobalt oxide nanoparticle, Heavy metals ion sensors

Received: 19 January 2024; Revised: 27 February 2024; Accepted: 13 March 2024; Published Online: 01 June 2024

[1] Nano-Structured Materials Processing Research Laboratory, Department of Electronics, Kavayitri Bahinabai Chaudhari, North Maharashtra University Jalgaon, MS 425001, India
[2] Department of Chemistry, Faculty of Science and Arts, and Promising Centre for Sensors and Electronic Devices (PCSED), Najran University, Najran-11001, Kingdom of Saudi Arabia
[3] Department of Materials Science and Engineering, The Ohio State University, Columbus 43210, OH, USA
[4] Department of Chemistry, Kavayitri Bahinabai Chaudhari, North Maharashtra University Jalgaon, MS 425001, India
[5] School of Semiconductor and Chemical Engineering, Jeonbuk National University, 567 Baekje-daero, Deokjin-gu, Jeonju 54896, Jeollabuk-do, Republic of Korea
[6] Department of Materials Science, University of Patras, 26504 Patras, Greece
*Author to whom correspondence should be addressed:
djshirale@nmu.ac.in (Dhammanand J. Shirale)
ahmadumar786@gmail.com (Ahmad Umar)

1. INTRODUCTION

Heavy metal ion contamination is one of the major issues that cause severe effects on human health and the environment. Among heavy metals, cadmium Cd^{2+} and Lead Pb^{2+} are notorious for being the world's most hazardous pollutants. For instance, the severity of Cd^{2+} and Pb^{2+} can lead to tubular dysfunction, bone degeneration, hypertension, altered normal gene expression, inhibiting DNA damage repair, inducing oxidative stress, and cancer [1-5]. Hence, it is essential to establish a highly sensitive, rapid, reliable, and cost-effective analytical technique for identifying and quantifying these heavy metal ions.

There are number of established analytical techniques for detecting heavy metals in natural water and the environment namely Hydride generation atomic fluorescence spectrometry (HG-AFS), Hydride generation atomic absorption spectroscopy (HG-AAS) [6], Inductively coupled plasma atomic emission spectroscopy (ICP-AES), Inductively coupled plasma mass spectrometry (ICP-MS) [7], Graphite furnace atomic absorption spectroscopy (GF-AAS) [8], and Fluorescence spectrometry. As the above listed detection techniques need sophisticated equipment, experienced personnel and a well-established laboratory setup making more expensive detection of heavy metals. Additionally, these methods are time-consuming, inaccessible, and unsuitable for field investigation. A simple, low-cost, portable, and accurate method for rapidly detecting or analyzing heavy metal ions in water and the environment is required. Electrochemical methods, particularly stripping voltammetry, have been determined to be the most advantageous approach because of its cheap development costs, high integration, and high sensitivity [9, 10].

Surface modification using nanoparticles or thin films is essential to enhance the performance of the sensor for electrochemical sensing applications, and this is being widely acknowledged. It is elucidated that the nanoscale materials have the shortest path for ion transport which provide efficacious and accurate detection with higher sensitivity and selectivity. [11]. Nanostructured metal oxides such as Zirconium oxide (ZrO_2), Vanadium oxide (V_2O_5), Zink oxide (ZnO), Iron oxide (Fe_3O_4), Tin oxide (SnO_2), Nickel oxide (NiO), and Cobalt oxide (CoOx) have been used widely in the detection of heavy metals [12-14] because of their multifunctional and interesting characteristics such as non-toxicity, biocompatibility, catalytic, sensing and other properties. Metal oxide nanoparticles have a high degree of crystallinity, a high surface-to-volume ratio, and a smooth electron transport path, making them a viable choice for many sensing applications. Recently, considerable attention has been drawn to cobalt oxides (CoOx), which show intriguing electrical, optical, electrochemical, and electrocatalytic properties. This is primarily because of its superior electrocatalytic activity toward heavy metal ions [15].

A single polypyrrole nanowire-based electrode decorated with cobalt oxide nanoparticles are used in this research to electrochemically determine heavy metal ions in potable water. The proven electrochemical sensing properties of polypyrrole modified CoOxNPs, namely efficient mass transfer, high surface area to volume ratio, and electro-catalysis heterostructures may exhibit lower detection limit and increased sensitivity for sensors.

2. EXPERIMENTAL DETAILS

2.1. Materials and Method

All reagents were analytical grade and purified further before use. Anodic aluminum oxide membrane (AAO) was purchased from Whatman International Ltd. (Maidstone, UK). The following chemicals were used in this study: Pyrrole (Sigma-Aldrich). lithium perchloric acid ($LiClO_4$) (USA), Sulphuric acid (H_2SO_4), hydrogen peroxide (H_2O_2) (Fisher Scientific (USA)), gold colloidal solution ($HAuCl_4$), cobalt chloride ($CoCl_2$) Sigma-Aldrich (AR-MED, Division of Quintiles Ltd. UK), phosphoric acid, Cadmium chloride $CdCl_2$ All reagents were prepared in Milli Q water 18M.

2.2. Preparation of cobalt oxide nanoparticles modified single polypyrrole nanowire electrode

The gold seeded AAO membrane was used to deposit polypyrrole thin film to make the polypyrrole nanowire of 6 μM in length. (Note: The entire process of making polypyrrole nanowire is discussed in our previously published paper [16, 17]). The polypyrrole nanowire was oriented and anchored via mask-less deposition between 3 μm gap of a gold pair of electrodes on a Si/SiO_2 wafer [18]. For the electrodeposition of cobalt oxide nanoparticles (CoOxNPs), the anchored polypyrrole nanowire (sPpyNW) electrode was immersed in a solution of 1 mM $CoCl_2$ and phosphate buffer (PBS - pH 7). The electrodeposition was carried out using cyclic voltammetry with potential between -1.2 and 1.1 V (for 10 cycles at scan rate of 100 mV/s) [19]. The deposited CoOxNPs/sPpyNW electrode was rinsed again with double distilled water and stored at room temperature (25 °C), in order to allow it dry. Field Emission Scanning Electron Microscopy (FESEM) and Energy Dispersive Spectroscopy (EDS) corroborate the deposition of CoOxNPs on sPpyNW. The Cadmium (Cd) and Lead (Pb) in potable water (either separately or mixed) was traced using a CoOxNPs-sPpyNW electrode in this study.

3. RESULTS AND DISCUSSION

3.1. Structural and elemental characterization of CoOxNPs modified sPpyNW

The structural and elemental characteristics of the cobalt oxide nanoparticles/single polypyrrole nanowire (CoOxNPs/sPpyNW) electrode were evaluated using Field Emission Scanning Electron Microscopy (FESEM) and Energy Dispersive X-ray Spectroscopy (EDS). The FESEM image, shown in the inset of Figure 1, illustrates the CoOx nanoparticles uniformly coating the sPpyNW at the nanometer scale. The EDS spectrum depicted in Figure 1 confirms the presence of cobalt oxide nanoparticles on the sPpyNW electrode. Peaks corresponding to cobalt (Co) and oxygen (O) validate the successful modification. Additionally, the silicon (Si) peak observed in the EDS spectrum is attributed to the silicon substrate used during sample preparation. The elemental percentage compositions are provided in the inset table of Figure 1. This comprehensive characterization supports the effective functionalization of the sPpyNW with CoOx nanoparticles. The modified nanowire electrode was subsequently employed to determine the concentrations of cadmium (Cd) and lead (Pb) in potable water, leveraging the enhanced sensitivity and specificity imparted by the CoOxNPs.

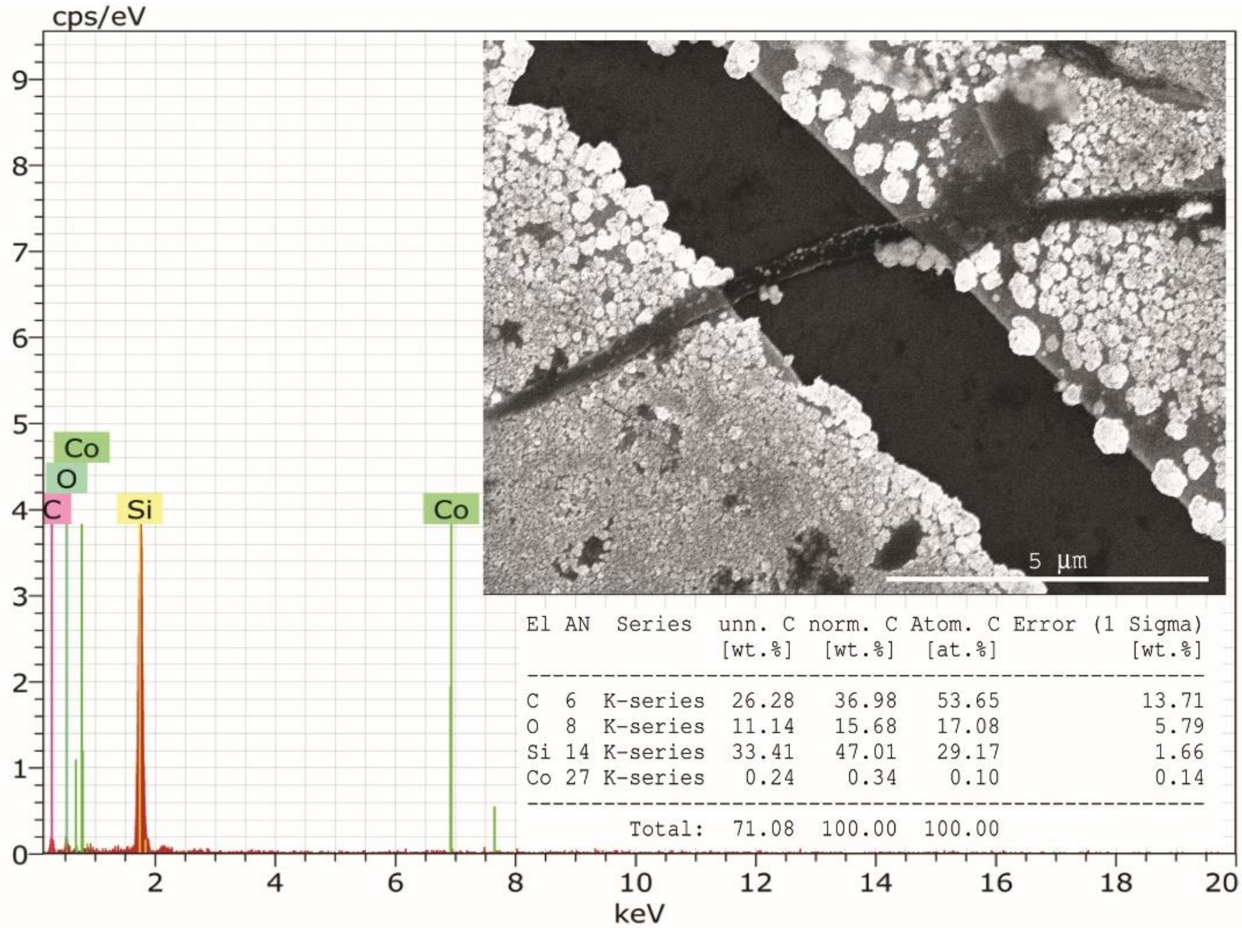

Fig. 1. EDS spectrum of Cobalt oxide nanoparticles decorated sPpyNW. Inset FESEM image of CoOxNPs/sPpyNW electrode and table of elemental composition.

3.2. Voltammetric study of CoOxNPs modified sPpyNW

A layer of cobalt oxide nanoparticles was decorated on the sPpyNW electrode by using cyclic voltammetry. Figure 2a. Depicts the cyclic voltammogram of the CoOx/sPpyNW electrode submerged in a solution containing 0.02 M of cobalt nitrate and 0.1 M acetate buffer solution (pH 7). As shown in Figures 2(a). A reduction peak developed at a negative potential of -0.8V, which corresponds to the reduction of Co^{2+} to Co [20, 21]. A tiny oxidation peak was detected on the reverse scan at a potential of -0.2 V, which may be ascribed to the removal of electrodeposited cobalt on the surface of polypyrrole nanowire.

The cyclic voltammogram of the CoOxNPs/sPpyNW electrode placed in alkaline solution confirms the deposition of cobalt oxide nanoparticles on the sPpyNW electrode surface. Figure 2(b). Shows cyclic voltammetric response of CoOxNPs/sPpyNW electrode placed in acetate buffer (pH 4.5), with applied potential in the range -1.1 to +1.3 V. In Figure 2(b) three redox peaks ascribed to various oxidation states of cobalt oxide particles. The electrochemical oxidation of aqueous Co (II) to Co_3O_4 observed at Ia/Ic redox pair, as seen in Figure 2(b) and the Equation 1. According to Equations 2 and 3 [22], another redox pair (IIa/IIc) can be attributed to the formation CoOOH. The pair of redox peaks seen at higher potentials (IIIa/IIIc) relate to the oxidation of CoOOH to CoO_2 as described in the following Equation 4. These results are consistent with earlier reports on the electrochemical performance of cobalt oxide nanoparticles [23, 15]

$$3Co(OH)_2 + 2OH^- \leftrightarrow Co_3O_4 + 4H_2O + 2e^- \quad (1)$$

$$Co_3O_4 + OH^- + H_2O \leftrightarrow 3CoOOH + e^- \quad (2)$$

$$Co(OH)_2 + OH^- \leftrightarrow CoOOH + H_2O + 2e^- \quad (3)$$

$$CoOOH + OH^- \leftrightarrow CoO_2 + H_2O + e^- \quad (4)$$

3.3. Electrochemical characterization of the CoOxNPs/ sPpyNW electrode

The cyclic voltammetric behavior of a cobalt oxide nanoparticles decorated polypyrrole nanowire CoOxNPs/sPpyNW electrode was investigated in the presence of 1 mM $K_3Fe(CN)_6$ in 0.1 M KCl as a standard redox couple across a potential range of -0.2 to 0.7 V at a scan rate of 100 mVs^{-1} as shown in Figure 2(c), because the sensor is reversible, it is capable of detecting target analyte in both oxidized and reduced states. There is a reversible interaction between the host and guest, thus the sensor surface is unaltered before and after the electrochemical scan is performed. The modified electrode's anodic peak current increased in comparison to the bare sPpyNW electrode, suggesting that the presence of cobalt oxide nanoparticles make ions more readily available at the electrode surface and accelerates electron transduction. The modifier creates a large number of active areas on the sensor's surface where excess analyte ions may accumulate.

Cyclic voltammetric measurements were performed to examine the scan rate influence on the redox reaction by changing the scan rate from 10 to 100 mV/s in a redox pair composed of 1 mM $K_3Fe(CN)_6$ in 0.1 M KCl as a supporting electrolyte. Peak currents rose as scan rates increased.

According to Figure 2(d), the redox peak current of the CoOxNPs/sPpyNW electrode was proportional to the square root of the scan rate, demonstrating that the CoOxNPs/sPpyNW electrode electrochemical reaction followed a typical diffusion-controlled mechanism [24]. It is worth mentioning that a direct relationship between peak current and bulk concentration was found as a result of the abundant active sites on the electrode surface interacting with all incoming ion molecules, which is a critical condition for an electrochemical sensor [25]. This property enables the CoOxNPs/sPpyNW electrode to be used effectively for the determination of Lead (Pb) and Cadmium (Cd).

3.4. Analytical performance of the CoOxNPs modified sPpyNW electrode.

3.4.1. Optimization of experimental conditions

Experimental conditions (Accumulation time, accumulation potential and supporting electrolyte) were established and optimized before constructing a calibration curve and finding a LOD of the CoOxNPs/sPpyNW electrode to produce a maximum peak current response, sharpness of the peak, and high repeatability. The test was carried out by adjusting each parameter separately while keeping others at their optimal values.

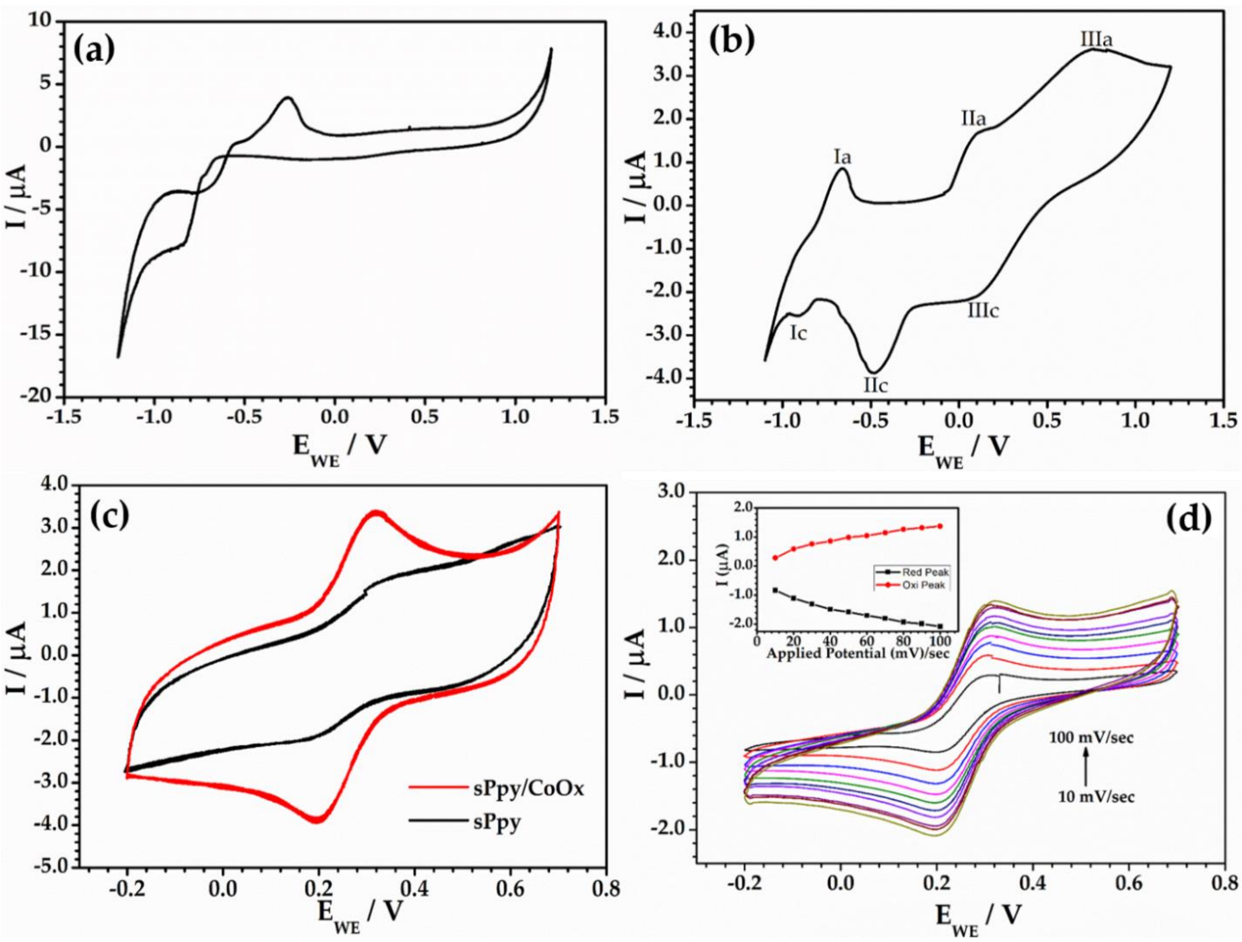

Fig. 2. **(a)** Cyclic voltammogram of deposited cobalt oxide nanoparticles on sPpyNW in 0.1 M acetate buffer solution containing 0.02 M cobalt nitrate in the potential range from -1.2 to 1.2V at 100mV/s scan rate. **(b)** Cyclic voltammogram (CV) response in 0.1M acetate buffer solution (without cobalt ions) in the potential range from -1.2 to 1.2V at 100mV/s scan rate, **(c)** CV responses of sPpyNW and CoOxNPs/sPpyNW at potential range -0.2 to 0.7V for scan rate of 100 mV/s. **(d)** CV response of CoOxNPs/sPpyNW electrode at different scan rates (scan rate/mV/s). Inset of **(b)** shows linear fitted plot of peak current vs scan rate.

The supporting electrolyte, pH value, deposition potential, and deposition duration were adjusted to get the optimum response of the proposed sensor for trace detection of Cd^{2+} and Pb^{2+} ions. The schematical representation of detection of Cd^{2+} and Pb^{2+} ions using the modified electrode is shown in Scheme 1. Scheme 1(a) corresponds to the response of modified sensor in absence of Cd^{2+} and Pb^{2+} ions. SW-ASV responses for 0.05 μM of Cd^{2+} and Pb^{2+} at pH 4.5 [26-28] were measured in four distinct supporting electrolytes: 0.1M HCL, 0.1M H_2SO_4, 0.1M KCL, and acetate buffer with 0.1M KCL (Figure 3(a)). For the H_2SO_4 solution, no noticeable peaks emerged at the same potential. In the HCL solution, just one peak was seen, and the peak of Cd^{2+} was not visible. Voltammetric peaks were found in KCL. However, well-defined voltammetric peaks for both ions were detected in 0.1M acetate buffer with KCL solution. As a result, in subsequent studies, a 0.1M acetate buffer and KCL solution was used. Figure 3(b) shows the influence of deposition potential on Cd^{2+} stripping reactions. The reaction signals rose remarkably when the deposition potentials were changed from -0.3 V to -1.5 V. The response for Cd^{2+} increased when the deposition potential shifted towards negative. The high response is recorded at -1.2 V. When the deposition potential was increased to -1.5 V, the current response was slightly dropped. This drop is most likely due to hydrogen evolution at -1.5 V potentials, and hydrogen bubbles may obstruct metal ion deposition at the electrode surface. The deposition potential was varied from −0.3V to −1.5V for a deposition time of 100 sec. As can be seen in Figure 3(c) the current density corresponding to the Pb^{2+} signal linearly increased to −1.5V. The influence of the deposition potential on the peak current of Cd^{2+} and Pb^{2+} after 100 sec accumulation was tested by keeping applied potential between -1.5 V to -0.3V (Figure 3(d)). The differences in Cd^{2+} and Pb^{2+} trends may be ascribed to the various standard potentials. The optimum accumulation potential for the following experiment was considered as -1.2V in order to achieve excellent sensitivity for both Cd^{2+} and Pb^{2+}.

The deposition time is another important aspect that determines the sensitivity of the result in stripping analysis. As shown in Figure 4(a), stripping current for Cd^{2+} rose almost linearly as the deposition duration increased from 10 to 100 seconds. The deposition duration was evaluated between 10 and 110 sec at a deposition potential of −1.2 V.

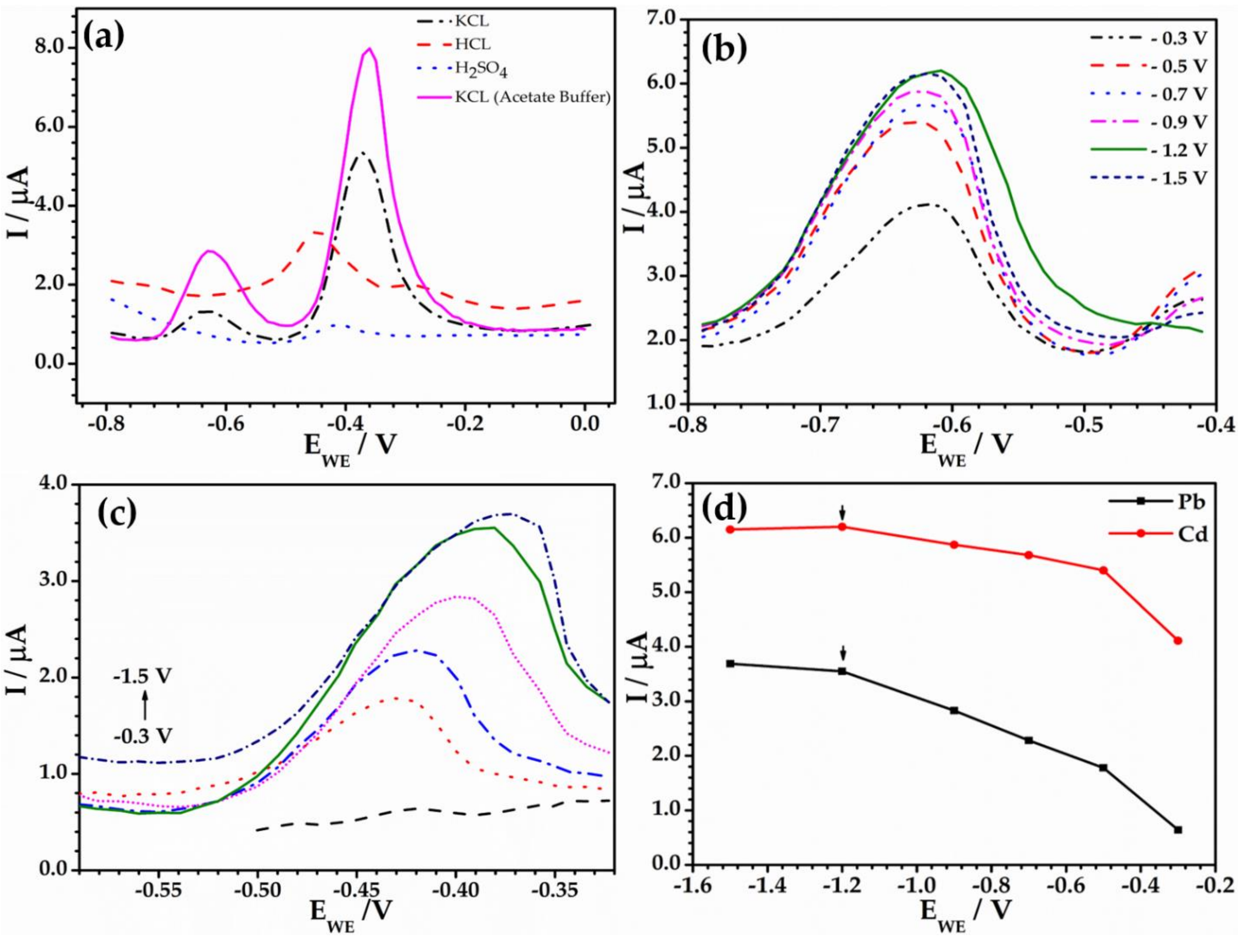

Fig. 3. Effect of a) Electrolyte b) SW-ASV response of 0.05 μM of Cd^{2+} for varying electrode deposition potential c) SW-ASV response of 0.05 μM of Pb^{2+} for varying electrode deposition potential d) Calibrated plot of deposition potential for Cd^{2+} and Pb^{2+} of peak current observed in SW-ASV.

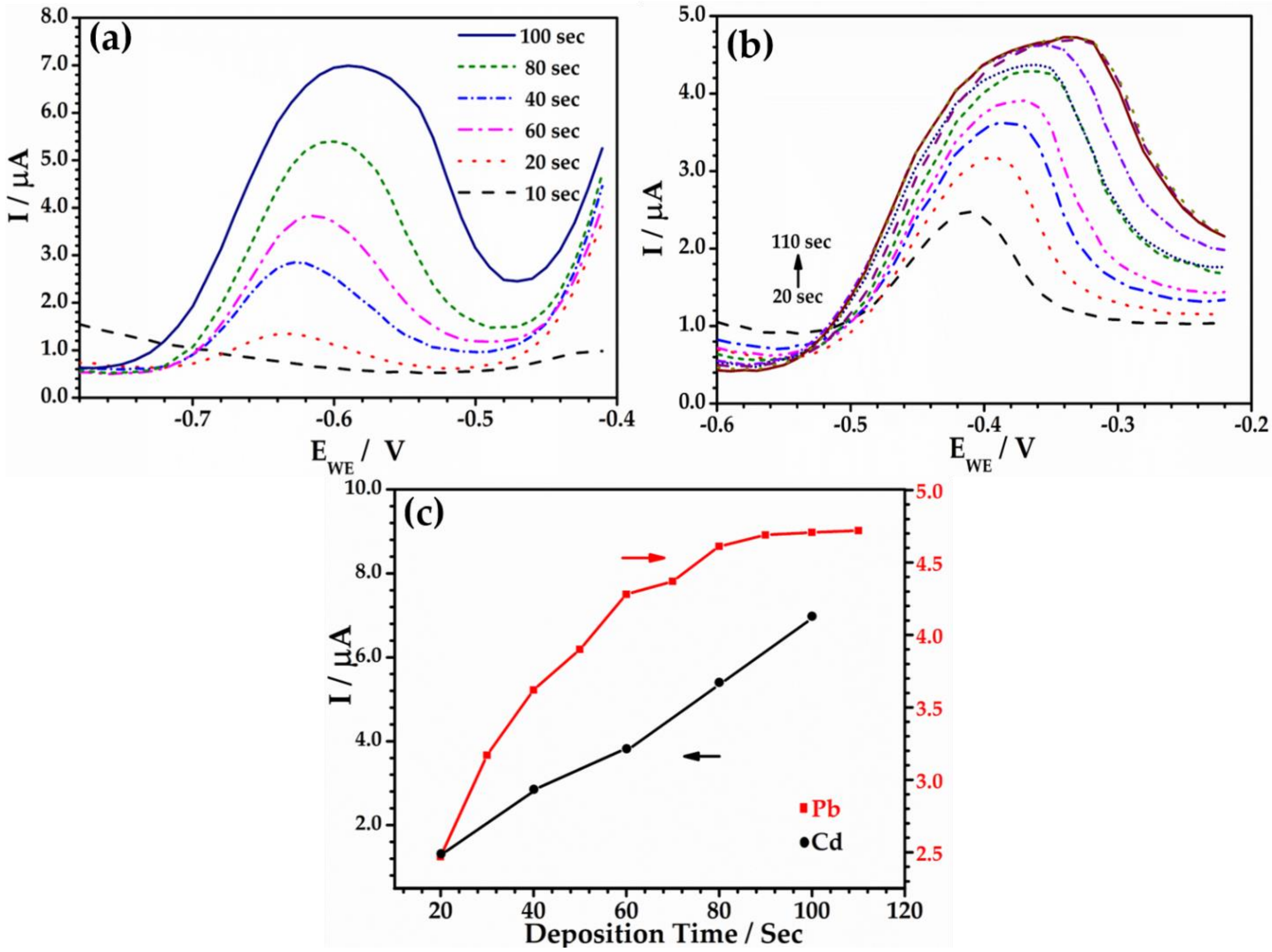

Fig. 4. (a) SW-ASV response of 0.05 µM of Cd^{2+} for varying electrode deposition time (b) SW-ASV response of 0.05 µM of Pb^{2+} for varying electrode deposition time (c) Calibrated plot of deposition time for the stripping response of 0.05 µM each of Pb^{2+} and Cd^{2+} ions.

Figure 4(b) shows that the Pb^{2+} signal increased up to 100 sec and then at 110 sec the stripping current response is almost same to the response of 100 sec. The impact of deposition duration on the peak currents of Cd^{2+} and Pb^{2+} was shown in Figure 4(c). Our findings show that when the deposition duration rose from 10 to 100 seconds, the response currents of Cd^{2+} and Pb^{2+} increased as well. The increased quantity of analyte on the modified electrode surface is responsible for this behavior. When the deposition duration was extended beyond 100 sec, no significant change in the stripping response of Cd^{2+} and Pb^{2+} was found, which was attributed to the electrode surface becoming saturated with large quantities of metal ions [29]. As a result, accumulation time of 100 s was chosen as the best option for achieving a larger response range while maintaining an acceptable detection limit.

3.4.2. Response of Cadmium (Cd) on CoOxNPs modified sPpyNW electrode in laboratory grade water

The proposed CoOxNPs/sPpyNW nanocomposites-modified electrode sensor was used to determine Cd^{2+} using the SW-ASV technique (Scheme 1(b)) under optimum circumstances. Figure 5(a) shows the electrode sensor's SW-ASV spectra as a function of Cd^{2+} concentration. The peak current of the electrode rises significantly as the concentration of Cd^{2+} increases, and the peak current reaches its maximum when the concentration of Cd^{2+} is raised to 0.1 µM. As shown in Figure 5(b), a plot of peak current intensity against Cd^{2+} concentration in the range of 0.00 to 0.11 µM showed a linear response ($R^2 = 0.9520$) with a relatively low detection limit of 0.22 μM, which is considerably lower than the drinking water standard.

The proposed technique's detection linearity range and limit were compared to other Cd^{2+} assays (Table 1), revealing that the new approach has higher or similar detection sensitivity. The low detection limit may be due to the CoOxNPs/sPpyNW nanocomposites' capacity to enrich for Cd^{2+}, showing that the produced CoOxNPs/sPpyNW nanocomposites-modified electrode sensor is effective at measuring low Cd^{2+} concentrations.

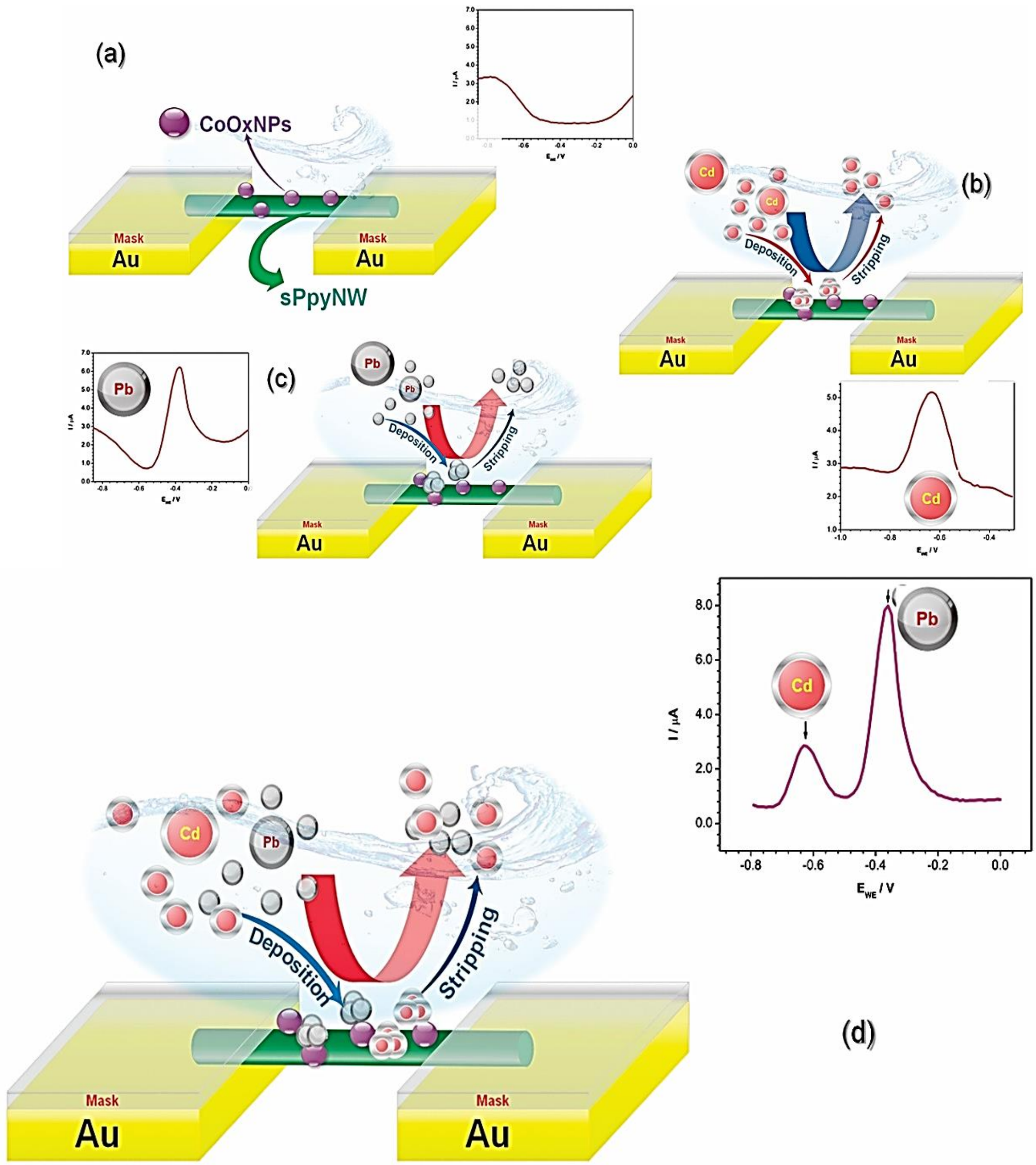

Scheme 1. Sensing mechanism of CoOxNPs/sPpyNW electrode (a) SW-ASV response of 0.00 µM of Cd^{2+} and Pb^{2+} in potable water (b) SW-ASV response of Cd^{2+} ions (c) SW-ASV response of Pb^{2+} ions (d) SW-ASV response of Cd^{2+} and Pb^{2+} in potable water.

3.4.3. Response of Lead (Pb) on CoOxNPs modified sPpyNW electrode in potable water

SW-ASV on CoOxNPs/sPpyNW electrode was used to perform quantitative Pb^{2+} detection (Scheme 1(c)) under ideal conditions. Figure 6(a) shows the SW-ASV responses at various Pb^{2+} concentrations ranging from 0 to 0.12 µM. The stripping peak currents increase as the Pb^{2+} concentration rises, and there is a good linear relationship between the concentrations of 0.01 µM and 0.12 µM. When the Pb^{2+} concentration was 0.00µM, the developed sensor had no response, and this concentration can be considered the sensor's quantification limit. The corresponding calibration plot, which plots the peak current vs. Pb^{2+} concentration, is shown in Figure 6(b). y= 48.396x +0.807 was the calibration plot equation, with 0.9723 as the correlation coefficient (R^2). The limit of detection (LOD) was calculated to be 0.013 µM, which is significantly lower (or comparable) than that of similar Pb^{2+} sensors.

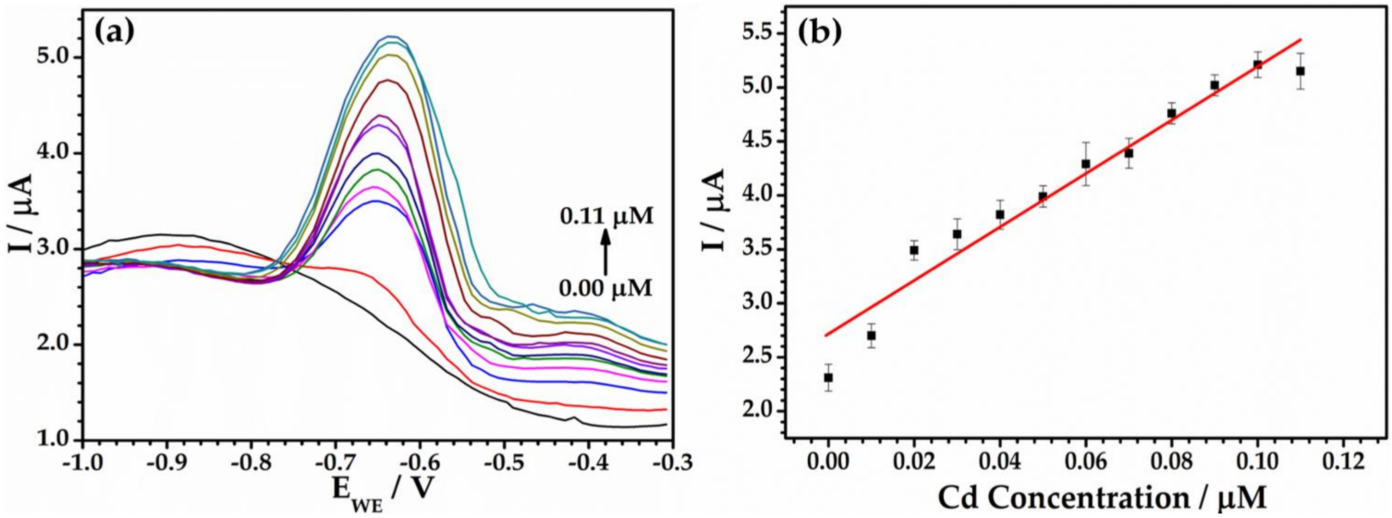

Fig. 5. (a) SW-ASV response of the CoOxNPs/sPpyNW electrode for 0.1 M acetate buffer and 0.1 M KCL presence of Cd^{2+} from 0 to 0.11 μM. (b) The calibration plot of peak current vs. Cd^{2+} concentrations.

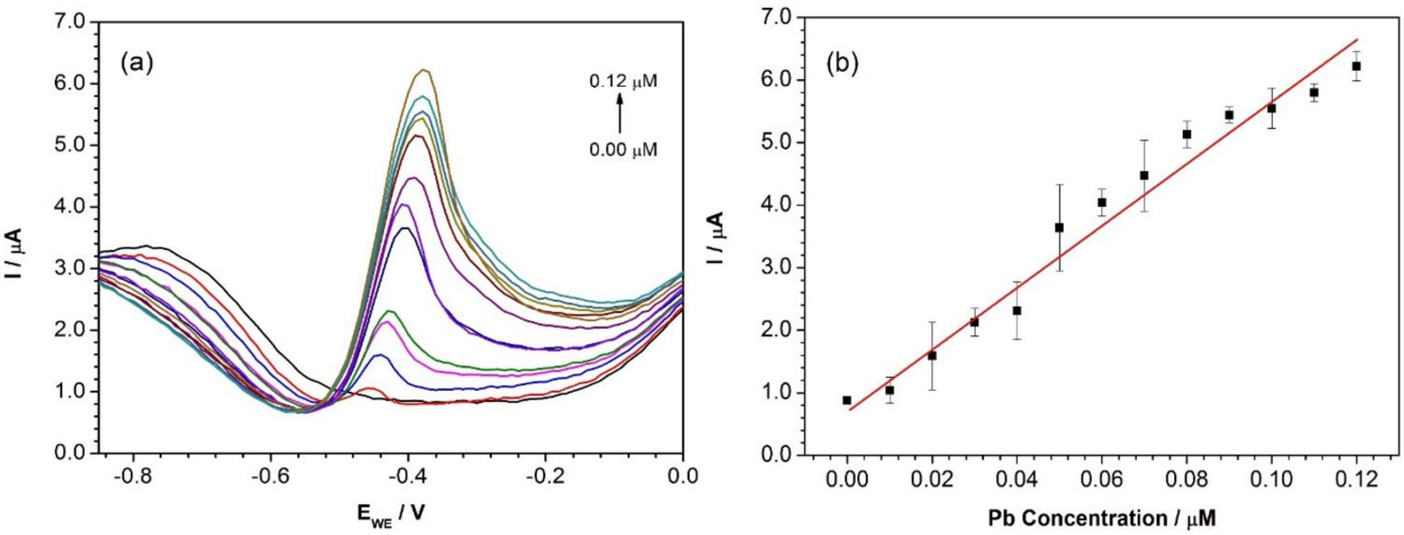

Fig. 6. (a) SW-ASV response of the CoOxNPs/sPpyNW electrode for 0.1 M acetate buffer and 0.1 M KCL presence of Pb^{2+} from 0 to 0.12 μM. (b) The calibration plot of peak current vs. Pb^{2+} concentrations.

3.5. Response of Cadmium (Cd) and Lead (Pb) together on CoOxNPs modified sPpyNW electrode in potable water

Along with individual Cd^{2+} and Pb^{2+} detection, we explored simultaneous Cd^{2+} and Pb^{2+} detection through SW-ASV using the same modified CoOxNPs/sPpyNW electrode (Scheme 1(d)) placed in 0.1 M acetate buffer and 0.1 M KCL solution at pH 4.5. The electrochemical responses of various concentrations of Cd^{2+} and Pb^{2+} have been studied using square wave anodic stripping voltammetry methods when both species are present in the same electrolytic solution. Cd^{2+} and Pb^{2+} were measured using -1.2 V and 100 sec deposition potentials, respectively. Figure 7(a) showed a series of SW-ASV responses when the concentrations of Cd^{2+} and Pb^{2+} were increased concurrently. For 0.01 μM Pb^{2+} solution, a stripping peak at -0.49 V was detected. Following the various concentration of Cd^{2+} and Pb^{2+} ions to the buffer solution, two distinct oxidation peaks at -0.49 V and -0.75 V were detected, corresponding to Cd^{2+} and Pb^{2+}, respectively. For all concentration responses, a peak separation of 260 mV between the two metal ions was found. As can be observed, both metal ions' peak current signal rises linearly with their concentration. Figure 7(b) shows the linear calibration curve for both metal ions. Cd^{2+} and Pb^{2+} have linear correlation coefficients of 0.8726 and 0.9468, respectively. The limit of detection can be found 0.026 μM and 0.013 μM for Cd^{2+} and Pb^{2+} respectively.

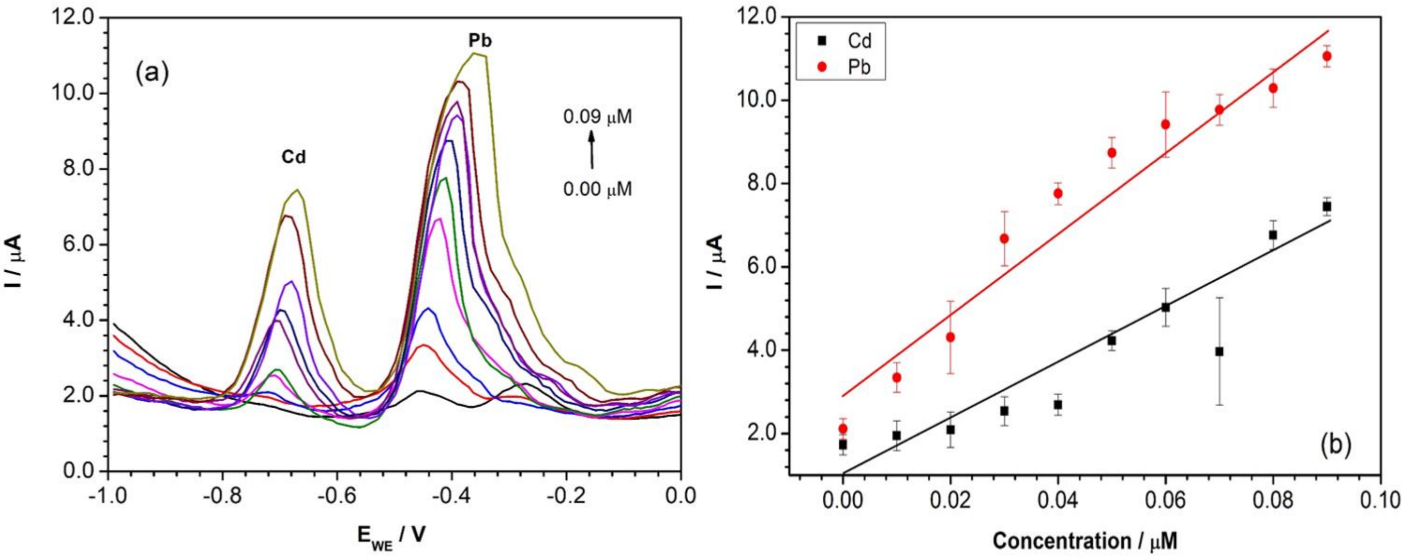

Fig. 7. (a) Striping voltammogram for the different concentrations of Cd^{2+} and Pb^{2+} on an in situ plated CoOxNPs/sPpyNW electrode in solution containing 0.1M acetate buffer + KCl. From bottom to top, 0.0 μM to 0.09 μM. (b) The calibration curve of Cd^{2+} and Pb^{2+}, respectively.

Table 1: Comparison of electrochemical performance of the electrodes for Voltammetric determination of Cadmium and Lead.

S. No.	Electrode	Method	LOD		Ref.
			Cd^{2+}	Pb^{2+}	
1	BiNP/Nafion/PGE	ASW	7.31	31.07	30
2	F-MWCNT/Fe_3O_4/ 0.5% Nafion/ GCE	SWV	1.57	1.74	31
3	Bi dendritic on glassy carbon H_2 template	SWASV	0.4	0.1	32
4	Bi/poly(p-ABSA)/ GCE	DPASV	0.63	0.80	33
5	CB–Nafion–GCE	DPASV	0.9	1.0	34
6	Ag-RDE	SASV	0.1	0.010	35
7	polyPCA/GE	SWASV	15.4	13.6	36
8	GCE-$MnCo_2O_4$ NPs	LSASV	0.79	1.67	37
9	NH_2 - Fe_3O_4@C/ GCE	SWASV	2.6	5.9	38
10	Sb-BDD	LSASV	38.1	25.4	39
11	BiBE	ASV	6.07	19.3	40
12	G/PANI/PS nanoporous fiber/SPCE	ASV	4.43	3.30	41
13	P(DPA-co-2ABN)/GC	DPASV	255	165	42
14	Diacetyldioxime/CPE	DPASV	4.48	2.07	43
15	PANI/ GC	SWASV	14.56	20.7	44
16	CoO_xNPs/PpyNW	SW-ASV	0.22 μM and 0.026 μM	0.013 μM and 0.013 μM	This Work

BiNP/Nafion/PGE: Bismuth nanoparticles and Nafion modified pencil graphite electrode; F-MWCNT/Fe_3O_4/0.5%Nafion/GCE: Magnetite nanoparticles and fluorinated multiwalled carbon nanotubes-modified glassy carbon electrode; CB–Nafion–GCE: Carbon black and Nafion (5 wt%)-modified glassy carbon electrode; Bi/poly (p-ABSA): Bismuth/poly(*p*-aminobenzene sulfonic acid) modified glassy carbon electrode; Ag-RDE: Silver rotating disk electrode; BiBE: Bismuth bulk electrode; GCE-MnCo2O4NPs: $MnCo_2O_4$ nanoparticles-modified Glassy carbon electrode; NH_2 - Fe_3O_4@C/GCE: Amino-functionalized Fe_3O_4@carbon microspheres-modified glassy carbon electrode; Sb-BDD: Antimony nanoparticle modified boron-doped diamond electrode; BiBE: Bismuth bulk electrode; P(DPA-co-2ABN); Poly(diphenylamine-co-2-aminobenzonitrile). GC; glassy carbon electrode; CPE; carbon paste electrode.

4. CONCLUSIONS

Square wave anodic stripping voltammetry (SW-ASV) for the determination of Cd^{2+} and Pb^{2+} in potable water individually and simultaneously using a sPpyNW electrode modified with CoOx nanoparticles (SW-ASV) was successfully carried out. FESEM and EDS confirms aligned sPpyNW and decorated Cobalt oxide nanoparticles, respectively. The electrochemical sensitivity in the detection of Cd^{2+} and Pb^{2+} is greatly improved by the large surface area and electrical conductivity of Cobalt oxide nanoparticles (CoOxNPs). The linear range for the detection of individual Cd^{2+} and Pb^{2+} ions was determined to be 0.00 to 0.11 µM for Cd^{2+} and 0.00 to 0.12 µM for Pb^{2+}, with detection limits of 0.22 µM ($R^2 = 0.9520$) for Cd^{2+} and 0.013 µM ($R^2 = 0.9723$) for Pb^{2+}. The linear range for simultaneous detection was determined to be 0.00 to 0.09 µM, with a detection limit of 0.026 µM (R^2 = 0. 8726) and 0.013 µM (R^2 = 0. 9468) for Cd^{2+} and Pb^{2+}, respectively.

CONFLICT OF INTEREST

The authors declare that there is no conflict of interests.

ACKNOWLEDGEMENT

Authors are thankful to the SERB DST, New Delhi, India, for the financial assistance under the Young Scientist scheme (SR/FTP/PS-041/2012). Authors are also thankful for financial assistance under the Scheme "Rajiv Gandhi Science & Technology Commission (RGS&TC), Government of Maharashtra" through 'Kavayitri Bahinabai Chaudhari North Maharashtra University, Jalgaon (KBCNMU/ RGSTC/ Sanction Order/34 (Project code No.: 35-LSR)), also for the fellowship sanctioned under "Teaching Associate Programme (TAP)" to Mr. Rahul S Salunke (NMU/11/TAP/24/2020).

REFERENCES

[1] Lin, J., Zhang, F. and Lei, Y., **2016.** Dietary intake and urinary level of cadmium and breast cancer risk: A meta-analysis. *Cancer epidemiology*, *42*, pp.101-107.

[2] Kim, H.N., Ren, W.X., Kim, J.S. and Yoon, J., **2012.** Fluorescent and colorimetric sensors for detection of lead, cadmium, and mercury ions. *Chemical Society Reviews*, *41*(8), pp.3210-3244.

[3] Zaouak, O., Authier, L., Cugnet, C., Castetbon, A. and Potin-Gautier, M., **2010.** Electroanalytical Device for Cadmium Speciation in Waters. Part 1: Development and Characterization of a Reliable Screen-Printed Sensor. *Electroanalysis: An International Journal Devoted to Fundamental and Practical Aspects of Electroanalysis*, *22*(11), pp.1151-1158.

[4] Goyer, R.A., Liu, J. and Waalkes, M.P., **2004.** Cadmium and cancer of prostate and testis. *Biometals*, *17*, pp.555-558.

[5] Xue, S., Shi, L., Wu, C., Wu, H., Qin, Y., Pan, W., Hartley, W. and Cui, M., **2017.** Cadmium, lead, and arsenic contamination in paddy soils of a mining area and their exposure effects on human HEPG2 and keratinocyte cell-lines. *Environmental research*, *156*, pp.23-30.

[6] Welna, M. and Pohl, P., **2017.** Potential of the hydride generation technique coupled to inductively coupled plasma optical emission spectrometry for non-chromatographic As speciation. *Journal of Analytical Atomic Spectrometry*, *32*(9), pp.1766-1779.

[7] Bradshaw, N., Hall, E.F. and Sanderson, N.E., **1989.** Communication. Inductively coupled plasma as an ion source for high-resolution mass spectrometry. *Journal of Analytical Atomic Spectrometry*, *4*(8), pp.801-803.

[8] Schlemmer, G. and Welz, B., **1986.** Palladium and magnesium nitrates, a more universal modifier for graphite furnace atomic absorption spectrometry. *Spectrochimica Acta Part B: Atomic Spectroscopy*, *41*(11), pp.1157-1165.

[9] Kumar Jena, B. and Retna Raj, C., **2008.** Gold nanoelectrode ensembles for the simultaneous electrochemical detection of ultratrace arsenic, mercury, and copper. *Analytical chemistry*, *80*(13), pp.4836-4844.

[10] Dutta, S., Strack, G. and Kurup, P., **2019.** Gold nanostar electrodes for heavy metal detection. *Sensors and Actuators B: Chemical*, *281*, pp.383-391.

[11] Li, C., Zhang, X., Wang, K., Zhang, H., Sun, X. and Ma, Y., **2014.** Dandelion-like cobalt hydroxide nanostructures: morphological evolution, soft template effect and supercapacitive application. *RSC Advances*, *4*(103), pp.59603-59613.

[12] Xu, R.X., Yu, X.Y., Gao, C., Jiang, Y.J., Han, D.D., Liu, J.H. and Huang, X.J., **2013.** Non-conductive nanomaterial enhanced electrochemical response in stripping voltammetry: The use of nanostructured magnesium silicate hollow spheres for heavy metal ions detection. *Analytica chimica acta*, *790*, pp.31-38.

[13] Dong, Y., Zhou, M. and Zhang, L., **2020.** Designed 3D porous core-shell vanadium oxide microspheres for the simultaneous electrochemical sensing of toxic metal ions. *Journal of Alloys and Compounds*, *827*, p.154357.

[14] Buica, G.O., Stoian, A.B., Manole, C., Demetrescu, I. and Pirvu, C., **2020.** Zr/ZrO_2 nanotube electrode for

detection of heavy metal ions. *Electrochemistry Communications*, *110*, p.106614.

[15] Noorbakhsh, A., Mirkalaei, M.M., Yousefi, M.H. and Manochehri, S., **2014.** Electrodeposition of Cobalt Oxide Nanostructure on the Glassy Carbon Electrode for Electrocatalytic Determination of para-Nitrophenol. *Electroanalysis*, *26*(12), pp.2716-2726.

[16] Salunke, R.S., Chavan, P.G. and Shirale, D.J., **2018.** Anodic stripping voltammetry studies of electrochemically engineered silver nanoparticles over single polypyrrole nanowire device for tracing of arsenic (III): An environmental perspective. *Nanotechnology for Environmental Engineering*, *3*(1), p.12.

[17] Salunke, R.S., Nakate, Y.T., Umar, A., Nakate, U.T., Ahmad, R. and Shirale, D.J., **2021.** Anodic stripping voltammetry analysis of gold nanoparticles functionalized one-dimensional single polypyrrole nanowire for arsenic sensing. *Surfaces and Interfaces*, *23*, p.100895.

[18] Shirale, D.J., Bangar, M.A., Chen, W., Myung, N.V. and Mulchandani, A., **2010.** Effect of aspect ratio (length: diameter) on a single polypyrrole nanowire FET device. *The Journal of Physical Chemistry C*, *114*(31), pp.13375-13380.

[19] Salimi, A., Mamkhezri, H., Hallaj, R. and Soltanian, S., **2008.** Electrochemical detection of trace amount of arsenic (III) at glassy carbon electrode modified with cobalt oxide nanoparticles. *Sensors and Actuators B: Chemical*, *129*(1), pp.246-254.

[20] Mendoza-Huizar, L.H., Robles, J. and Palomar-Pardavé, M., **2002.** Nucleation and growth of cobalt onto different substrates: Part I. Underpotential deposition onto a gold electrode. *Journal of Electroanalytical Chemistry*, *521*(1-2), pp.95-106.

[21] Palomar-Pardavé, M., González, I., Soto, A.B. and Arce, E.M., **1998.** Influence of the coordination sphere on the mechanism of cobalt nucleation onto glassy carbon. *Journal of Electroanalytical Chemistry*, *443*(1), pp.125-136.

[22] Spataru, N., Terashima, C., Tokuhiro, K., Sutanto, I., Tryk, D.A., Park, S.M. and Fujishima, A., **2003.** Electrochemical behavior of cobalt oxide films deposited at conductive diamond electrodes. *Journal of the Electrochemical Society*, *150*(7), p.E337.

[23] Hallaj, R., Akhtari, K., Salimi, A. and Soltanian, S., **2013.** Controlling of morphology and electrocatalytic properties of cobalt oxide nanostructures prepared by potentiodynamic deposition method. *Applied surface science*, *276*, pp.512-520.

[24] Jokinen, M., Manzanares, J.A. and Murtomäki, L., **2019.** Thermodiffusion of sodium polystyrene sulfonate in a supporting electrolyte. *Electrochimica Acta*, *317*, pp.542-550.

[25] Chen, D., Zhuang, X., Zhai, J., Zheng, Y., Lu, H. and Chen, L., **2018.** Preparation of highly sensitive Pt nanoparticles-carbon quantum dots/ionic liquid functionalized graphene oxide nanocomposites and application for H_2O_2 detection. *Sensors and Actuators B: Chemical*, *255*, pp.1500-1506.

[26] Durai, L. and Badhulika, S., **2020.** Simultaneous sensing of copper, lead, cadmium and mercury traces in human blood serum using orthorhombic phase aluminium ferrite. *Materials Science and Engineering: C*, *112*, p.110865.

[27] Wang, J., Lu, J., Hocevar, S.B., Farias, P.A. and Ogorevc, B., **2000.** Bismuth-coated carbon electrodes for anodic stripping voltammetry. *Analytical chemistry*, *72*(14), pp.3218-3222.

[28] Ghazali, N.N., Mohamad Nor, N., Abdul Razak, K., Lockman, Z. and Hattori, T., **2020.** Hydrothermal synthesis of bismuth nanosheets for modified APTES-functionalized screen-printed carbon electrode in lead and cadmium detection. *Journal of Nanoparticle Research*, *22*, pp.1-11.

[29] Gao, X., Wei, W., Yang, L. and Guo, M., **2006.** Carbon Nanotubes/Poly (1, 2-diaminobenzene) nanoporous composite film electrode prepared by Multipulse Potentiostatic Electropolymerisation and its application to determination of trace heavy metal ions. *Electroanalysis: An International Journal Devoted to Fundamental and Practical Aspects of Electroanalysis*, *18*(5), pp.485-492.

[30] Palisoc, S., Gonzales, A.J., Pardilla, A., Racines, L. and Natividad, M., **2019.** Electrochemical detection of lead and cadmium in UHT-processed milk using bismuth nanoparticles/Nafion®-modified pencil graphite electrode. *Sensing and Bio-Sensing Research*, *23*, p.100268.

[31] Li, Y., Huang, H., Cui, R., Wang, D., Yin, Z., Wang, D., Zheng, L., Zhang, J., Zhao, Y., Yuan, H. and Dong, J., **2021.** Electrochemical sensor based on graphdiyne is effectively used to determine Cd^{2+} and Pb^{2+} in water. *Sensors and Actuators B: Chemical*, *332*, p.129519.

[32] Scandurra, A. and Mirabella, S., **2021.** Square wave anodic stripping voltammetry applied to a nano-electrode for trace analysis of Pb (II) and Cd (II) ions in

solution. *IEEE Sensors Journal*, *21*(20), pp.22134-22142.

[33] Wu, Y., Li, N.B. and Luo, H.Q., **2008.** Simultaneous measurement of Pb, Cd and Zn using differential pulse anodic stripping voltammetry at a bismuth/poly (p-aminobenzene sulfonic acid) film electrode. *Sensors and Actuators B: Chemical*, *133*(2), pp.677-681.

[34] Xie, R., Zhou, L., Lan, C., Fan, F., Xie, R., Tan, H., Xie, T. and Zhao, L., **2018.** Nanostructured carbon black for simultaneous electrochemical determination of trace lead and cadmium by differential pulse stripping voltammetry. *Royal Society open science*, *5*(7), p.180282.

[35] Bonfil, Y. and Kirowa-Eisner, E., **2002.** Determination of nanomolar concentrations of lead and cadmium by anodic-stripping voltammetry at the silver electrode. *Analytica Chimica Acta*, *457*(2), pp.285-296.

[36] Lima, T.M., Soares, P.I., do Nascimento, L.A., Franco, D.L., Pereira, A.C. and Ferreira, L.F., **2021.** A novel electrochemical sensor for simultaneous determination of cadmium and lead using graphite electrodes modified with poly (p-coumaric acid). *Microchemical Journal*, *168*, p.106406.

[37] Antunović, V., Ilić, M., Baošić, R., Jelić, D. and Lolić, A., **2019.** Synthesis of $MnCo_2O_4$ nanoparticles as modifiers for simultaneous determination of Pb (II) and Cd (II). *PloS one*, *14*(2), p.e0210904.

[38] Bai, F., Zhang, X., Hou, X., Liu, H., Chen, J. and Yang, T., **2019.** Individual and simultaneous voltammetric determination of Cd (II), Cu (II) and Pb (II) applying amino functionalized Fe_3O_4@ carbon microspheres modified electrode. *Electroanalysis*, *31*(8), pp.1448-1457.

[39] Toghill, K.E., Xiao, L., Wildgoose, G.G. and Compton, R.G., **2009**. Electroanalytical determination of cadmium (II) and lead (II) using an antimony nanoparticle modified boron-doped diamond electrode. *Electroanalysis: An International Journal Devoted to Fundamental and Practical Aspects of Electroanalysis*, *21*(10), pp.1113-1118.

[40] Armstrong, K.C., Tatum, C.E., Dansby-Sparks, R.N., Chambers, J.Q. and Xue, Z.L., **2010.** Individual and simultaneous determination of lead, cadmium, and zinc by anodic stripping voltammetry at a bismuth bulk electrode. *Talanta*, *82*(2), pp.675-680.

[41] Promphet, N., Rattanarat, P., Rangkupan, R., Chailapakul, O. and Rodthongkum, N., **2015.** An electrochemical sensor based on graphene/polyaniline/polystyrene nanoporous fibers modified electrode for simultaneous determination of lead and cadmium. *Sensors and Actuators B: Chemical*, *207*, pp.526-534.

[42] Philips, M.F., Gopalan, A.I. and Lee, K.P., **2012.** Development of a novel cyano group containing electrochemically deposited polymer film for ultrasensitive simultaneous detection of trace level cadmium and lead. *Journal of hazardous materials*, *237*, pp.46-54.

[43] Hu, C., Wu, K., Dai, X. and Hu, S., **2003.** Simultaneous determination of lead (II) and cadmium (II) at a diacetyldioxime modified carbon paste electrode by differential pulse stripping voltammetry. *Talanta*, *60*(1), pp.17-24.

[44] Wang, Z., Liu, E. and Zhao, X., **2011.** Glassy carbon electrode modified by conductive polyaniline coating for determination of trace lead and cadmium ions in acetate buffer solution. *Thin Solid Films*, *519*(15), pp.5285-5289.

